Title: Generation of Orientation-Independent Response Spectrum Matched Records Satisfying Minimum Fourier Amplitude and Power Spectral Density Requirements

Running Title: Bidirectional Spectral Matching

Author: Luis A. Montejo, PhD, PE

Affiliation: Department of Engineering Sciences and Materials, College of Engineering, University of Puerto Rico at Mayagüez, Mayagüez, PR 00681, Puerto Rico

Email: luis.montejo@upr.edu

Preprint Status Statement: This is a non-peer-reviewed preprint submitted to EarthArXiv. This manuscript is currently under peer review at *Earthquake Spectra*.

Generation of Orientation-Independent Response Spectrum Matched Records Satisfying Minimum Fourier Amplitude and Power Spectral Density Requirements

Luis A. Montejo, PhD, PE[1]

Abstract

The seismic design and assessment of critical infrastructure, particularly within the nuclear industry, relies heavily on acceleration time histories compatible with a Design Response Spectrum (DRS). While current spectral matching algorithms effectively tune ground motions to match a target DRS, this process can inadvertently deplete the signal's energy at specific frequencies, leading to unstable and unconservative In-Structure Response Spectra (ISRS). To mitigate this, the U.S. Nuclear Regulatory Commission (US-NRC) Standard Review Plan (SRP) 3.7.1 mandates a secondary check ensuring the motion satisfies a minimum Power Spectral Density (PSD) requirement. However, while modern seismic hazard definitions have shifted toward orientation-independent metrics (RotDnn), existing matching tools address PSD compliance only for single components. This article presents a unified algorithm that modifies bi-directional seed records to simultaneously match a target RotDnn response spectrum and satisfy minimum RotDnn Fourier Amplitude Spectrum (FAS) and PSD requirements. The methodology integrates the Continuous Wavelet Transform (CWT) with an iterative multi-stage scaling process—combining global frequency adjustments for FAS compliance with localized time-domain gains for PSD sufficiency. This approach allows for the generation of records that meet strict regulatory energy criteria while preserving most of the non-stationary characteristics and directionality of the seed motions.

Keywords: Orientation-independent ground motion, bi-directional shaking, time-history analysis, seismic input selection, decision trees.

1. Introduction

Dynamic time history analysis has become a cornerstone of performance-based seismic design and the safety assessment of critical infrastructure. For nuclear facilities, where safety margins must be rigorously quantified, the selection and modification of input ground motions are strictly regulated. The U.S. Nuclear Regulatory Commission (US-NRC) Standard Review Plan (SRP) 3.7.1 [1] and industry standards such as ASCE 4-16 [2] require that input motions generate response spectra that closely match the Design Response Spectra (DRS). While spectral matching—the process of modifying a recorded motion to match a smooth target spectrum—is the standard solution for generating these inputs, it introduces significant signal processing challenges that can compromise the validity of the structural response.

Historically, spectral matching was performed in the frequency domain, where the Fourier amplitudes of a seed record were adjusted to match the target spectrum while preserving phase angles. However, this approach often distorts the non-stationary characteristics of the ground

[1] Call Box 9000, Dept. of Engineering Sciences and Materials, University of Puerto Rico at Mayaguez, Mayaguez, PR 00680-9000. luis.montejo@upr.edu

motion, producing unrealistic energy distributions and overestimating the number of strong motion cycles [3]. To mitigate these issues, time-domain adjustment methods were developed, initially by [4,5] and later refined in widely used algorithms such as RspMatch [6–8] and the recent Greedy Wavelet Method (GWM) [9]. These approaches modify the acceleration time history by iteratively adding limited-duration wavelets to the seed motion at specific times and frequencies to correct spectral mismatches.

Distinct from these additive time-domain methods is the time-frequency approach based on the Continuous Wavelet Transform (CWT) [10–12]. Rather than superimposing new wavelets onto the record, this method decomposes the seed motion into detail functions (time-frequency atoms). These functions are analogous to the infinite sinusoids in the Fourier transform; however, in contrast to Fourier sinusoids which possess constant amplitude and infinite duration, the detail functions are finite and localized in time. The detail functions are then iteratively scaled—rather than summed—before being reconstructed via the Inverse Continuous Wavelet Transform (ICWT). This decomposition-scaling approach is particularly effective at preserving the non-stationary evolution of the seed record, as it modifies the intensity of the existing energy packets rather than introducing artificial ones.

Despite the efficacy of these modern matching algorithms, a critical artifact remains: the "tight" matching of a response spectrum (PSA) can inadvertently deplete the signal's energy at specific frequency bands [13,14]. Because the response spectrum represents the peak response of a Single Degree of Freedom (SDOF) oscillator, and that response is influenced by a wide frequency range—not merely the frequency corresponding to the SDOF's natural vibration [15,16]—a record can generate the required peak spectral response while lacking sufficient total energy or power at that frequency. This deficiency is particularly dangerous for the generation of In-Structure Response Spectra (ISRS). Previous studies [17–19] have demonstrated that enveloping the design PSA is necessary but not sufficient, as input motions matched solely to the PSA can lead to unstable and potentially unconservative mean ISRS estimates. To guard against this, US-NRC SRP 3.7.1 imposes a secondary acceptance criterion: the Power Spectral Density (PSD) of the input motion must exceed a minimum target function.

While the minimum PSD requirement ensures energy sufficiency, its implementation has lagged behind the evolution of seismic hazard definitions. Modern ground motion models and design codes (e.g., ASCE 7-22 [20]) have shifted toward orientation-independent metrics, specifically the period-dependent maximum rotated component (RotD100) [21]. This shift complicates the matching process significantly. Unlike single-component matching, satisfying a RotD100 target requires the simultaneous modification of two orthogonal horizontal components such that their combined response at all angles meets the target. While methodologies have been proposed to achieve tight RotDnn PSA matches [22,23] and to construct target PSDs compatible with RotDnn spectra [24], there is a lack of algorithms capable of modifying seed records to match these targets. This article addresses this gap by presenting a unified algorithm based on the CWT decomposition framework. The proposed method modifies bi-directional seed records to simultaneously satisfy a tight RotDnn PSA match and minimum RotDnn Fourier Amplitude Spectrum (FAS) and PSD requirements. By integrating global frequency adjustments with localized power injection, the

algorithm meets strict nuclear safety criteria while preserving the non-stationary characteristics and directionality of the seed motions.

2. Methodology

The proposed algorithm modifies a pair of orthogonal seed acceleration time histories, $a_1(t)$ and $a_2(t)$, to simultaneously satisfy three objective functions: (1) a tight match to a target RotDnn response spectrum PSA_{target}, (2) compliance with a minimum RotDnn Fourier Amplitude Spectrum (FAS_{target}), and (3) compliance with a minimum RotDnn Power Spectral Density (PSD_{target}).

The primary target, PSA_{target}, is typically defined by the applicable design code, ground motion models for specific scenarios, or a Probabilistic Seismic Hazard Analysis (PSHA). The corresponding compatible target RotDnn FAS and PSD functions can be generated following the methodology proposed in [24]. The modification procedure relies on the Continuous Wavelet Transform (CWT) to decompose the signals into the time-frequency domain, modify their energy content at specific scales and times, and reconstruct them into time histories. The algorithm is organized into three sequential stages.

2.1 The CWT Framework

The core modification engine utilizes the CWT with the impulse response wavelet proposed in [12]:

$$\Psi(t) = e^{-\zeta\Omega|t|} sin(\Omega t) \tag{1}$$

where ζ and Ω are parameters defining the shape (localization) and central frequency of the wavelet, respectively. Values of $\zeta=0.05$ and $\Omega=\pi$ have been used successfully in the past for spectral matching purposes.

At a fixed scale s_j and time position p_k, the wavelet coefficient $C(s_j,p_k)$ of the acceleration history $a(t)$ sampled at N intervals equally spaced at Δt, is obtained via the convolution of the signal with the wavelet function ψ:

$$C(s_j, p_k) \sim \frac{\Delta t}{\sqrt{s_j}} \sum_{k=1}^{N} a(t) \Psi\left(\frac{t - p_k}{s_j}\right) \tag{2}$$

The resulting matrix of coefficients $C(s_j,p_k)$ maps the energy density of the signal in the time-scale domain, where the scale s is inversely proportional to frequency. The original time history can be recovered using the Inverse Continuous Wavelet Transform (ICWT). For numerical implementation, this is approximated as a summation over discrete scales:

$$a(t) \sim \frac{1}{K_\psi} \sum_j \left[\frac{\Delta p}{s_j^{5/2}} \sum_{k=1}^{N} C(s_j, p_k) \Psi\left(\frac{t - p_k}{s_j}\right) \right] = \frac{1}{K_\psi} \sum_j D_j(t) \tag{3}$$

where K_ψ is a reconstruction constant specific to the analyzing wavelet. The term within the brackets represents the detail function $D_j(t)$ at scale s_j. For the impulse response wavelet, the relation between s_j and the predominant frequency (f_j) in Hz and period (T_j) is given by equation

4. Further details on the mathematical properties and advantages of this wavelet in the analysis of earthquakes records are discussed in [7,12].

$$f_j = \frac{\Omega}{2\pi}\frac{1}{s_j} \qquad T_j = \frac{2\pi}{\Omega}s_j \tag{4}$$

For this application the scale vector is defined to adapt automatically to the seed record sampling frequency (f_s) and total duration (T_{tot}). The scales correspond to 300 frequency values logarithmically spaced between min($4/T_{tot}$, 0.1Hz) and the Nyquist frequency ($f_s/2$). The $4/T_{tot}$ lower bound allows that at least 4 cycles of the lowest frequency (longest period) analyzed fit within the record duration to ensure proper reconstruction of long duration records. The detail functions are the fundamental "atoms" of the spectral matching algorithm; while they are localized in time and not purely harmonic, they exhibit a dominant frequency corresponding to scale s_j. The proposed algorithm operates by scaling these detail functions $D_j(t)$ rather than adding external wavelets, thereby preserving most of the temporal structure of the seed motion.

2.2 Stage I: RotDnn Response Spectrum Matching

The first stage aims to match the orientation-independent target response spectrum. This is accomplished using the iterative CWT-based algorithm proposed in [22]. The seed record is first amplitude scaled to reduce the initial misfit with the target response spectrum. The scale factor is computed as the ratio of the "area" (sum of ordinates) under PSA_{target} to the "area" under the seed RotD100 spectrum, strictly within the matching frequency range. For the cases presented in this work the response spectrum matching range was fixed at [0.2Hz-50Hz]. Notice this is the range where the spectral matching would be verified, which is different than the frequency range used to decompose the record discussed in the previous section.

Once the initial amplitude scaling is performed, the iterative scaling of the detail functions of both horizontal components is performed simultaneously. At each iteration i, the RotDnn spectrum of the current pair of records (PSA_i^{RotDnn}) is computed. For every frequency f_j, a scaling factor γ_j is computed:

$$\gamma_j = \frac{PSA_{target}(f_j)}{PSA_i^{RotDnn}(f_j)} \tag{5}$$

Each of these frequency-dependent scaling factors is applied to the corresponding detail functions $D_j(t)$ of both orthogonal components. This operation is repeated until a tight match to the target response spectrum is attained. By applying the same scalar to both components, the relative amplitude and phase relationship between $a_1(t)$ and $a_2(t)$ is preserved, maintaining most of the natural directionality of the ground motion. Further details on the computational implementation are comprehensively detailed in [22].

2.3 Stage II: Minimum RotDnn FAS Compliance

Upon convergence of the response spectrum, the algorithm performs a global energy check in the frequency domain. The RotDnn Fourier Amplitude Spectrum (FAS^{RotDnn}) of the matched pair is computed and compared against a minimum requirement, typically defined as a fraction α of the

target FAS. This comparison is performed within a frequency range of interest; for the numerical examples in this work this range was set as [0.3Hz-30Hz]. These frequency ranges would vary depending on the specific structure and site characteristics. Notice that this range is different (narrower) than the range used to verify the response spectrum match. For optimal algorithm performance, the response spectrum range shall – at least - enfold the FAS and PSD ranges.

Notice also that SRP 3.7.1 does not require a FAS check (only PSD); however, this was devised as a useful intermediate step in the matching process, as the same process to estimate the target PSD provides also a target FAS as an intermediate step [24]. To be consistent with the PSD minimum threshold of 0.7 in SPR 3.7.1, the FAS inferior limit was set at $\sim\sqrt{0.7}$ (0.84).

While both are based on the iterative scaling of the detail functions, this secondary adjustment stage for FAS differs fundamentally from the primary response spectral matching in both intent and execution. While the response spectral matching (Stage 1) aims to tightly fit the target spectrum globally, minimizing the error across all frequencies, the FAS adjustment (Stage 2) is strictly a conditional process designed to satisfy a minimum inequality constraint (e.g., $FAS^{RotDnn} \geq 84\%$ of target). It does not attempt to match the target curve exactly; rather, it acts as a "floor," engaging only when the signal's energy falls below the designated threshold.

The execution mechanism further distinguishes the two processes. In response spectral matching, the detail functions at *all* scales of interest are modified simultaneously in every iteration to converge quickly on the target. In contrast, the FAS adjustment employs a sequential, "surgical" approach: each iteration identifies only the single most critical frequency where the spectral deficiency is greatest. A scaling factor is applied exclusively to the detail function corresponding to that specific frequency's scale, leaving all other scales untouched. The signal is then reconstructed, and a new critical frequency is identified in the subsequent iteration. While this iterative, point-by-point process is computationally more intensive and time-consuming, it is essential for ensuring that modifications remain localized, thereby minimizing disruption to the rigorous response spectral match established in the previous stage.

2.4 Stage III: Localized RotDnn PSD Adjustment

The Power Spectral Density (PSD) adjustment process (Stage 3) follows a conditional, iterative logic similar to the FAS adjustment but introduces a critical temporal constraint to address energy concentration. Like the FAS stage, it is triggered only if the minimum RotD100/Target ratio falls below a specified threshold (e.g., 0.70) within the frequency range of interest (e.g., [0.3Hz–30Hz]). It also employs the same "surgical" approach: each iteration identifies the single most critical frequency where the deficiency is greatest and computes a scaling factor to lift the spectral amplitude at that specific scale.

However, the execution differs fundamentally in the time domain to account for the definition of PSD as power (energy per unit time). While the FAS adjustment applies a constant scaling factor across the entire record duration for a given frequency scale, the PSD adjustment modulates this factor using a time-domain window (e.g., Tukey) centered on the strong motion duration ($SD_{5\text{-}75}$). This ensures that the added energy is not distributed arbitrarily across the record's tail or quiet periods but is concentrated within the significant shaking phase. This localization preserves the

non-stationary envelope of the acceleration history while effectively increasing the signal's power density to meet the target requirements.

2.5 Final Adjustments

After the spectral adjustments are complete, the algorithm applies a final post-processing sequence to ensure the generated records are both physically realistic and strictly compliant. First, a baseline correction is implemented. This correction involves removing a low-order polynomial trend from the acceleration time series and employing a targeted scheme that specifically adjusts the beginning and end of the signal to zero-out residual velocities and displacements while preserving the strong motion portion. This scheme was originally proposed in [25] and a detailed outline of the algorithm is provided in [26].

Because baseline correction can slightly alter the signal's energy content—potentially pushing a borderline record out of compliance—a final scalar amplification factor is computed. This factor is determined through a constraint-based check that calculates the minimum scaling required to re-satisfy the lower-bound thresholds for both the FAS and PSD. However, this additional gain is strictly constrained to prevent the response spectral match from exceeding the upper tolerance limit (e.g., 1.3 times the target). Consequently, the final scaling represents a balanced compromise: maximizing compliance with minimum energy requirements (FAS/PSD) only to the extent permitted by the maximum tolerance for response spectral misfit.

3. Numerical example

The algorithm described in Section 2 has been implemented in an open-source Python library that is freely available online. The numerical results presented in this section were generated using this implementation.

3.1 Target Spectra

The target response spectrum (PSA_{target}) was established as a site-specific spectrum developed using the BSSA14 ground motion model [27] for a strike-slip earthquake with moment magnitude M_w 7, a Joyner–Boore distance (R_{JB}) of 50 km, and a 30m average shear-wave velocity (VS_{30}) of 400 m/s. The resulting RotD50 spectrum was subsequently converted into a RotD100 spectrum utilizing the period-dependent ratios proposed by [28]. The corresponding target RotD100 FAS and PSD functions [24] were constructed assuming a significant strong motion duration $SD_{5\text{-}75}$ of 10.4 s [29].

The frequency range for PSA matching was set to 0.2–50 Hz, while the range for satisfying minimum FAS and PSD requirements was set to 0.3–30 Hz. The allowable matching tolerances follow the recommendations of SRP 3.7.1: between 0.9 and 1.3 for the PSA match, and greater than 0.7 for the minimum PSD check. To maintain consistency with the PSD minimum threshold, the lower limit for the FAS was set at ~$\sqrt{0.7}$ (0.84).

3.2 Seed Record and Initial Amplitude Scaling

Seed record selection is a critical step in any spectral matching methodology; it is advantageous to select a seed from an event with similar site characteristics and a response spectral shape that

already approximates the target. The seed record selected for this example is from the 1999 M_w 6.2 Chi-Chi (Taiwan) earthquake (RSN2988 from the NGA-West2 database [30]).
Figure 1 displays the spectra of the initial seed and the amplitude-scaled record alongside the target spectra and the specified limits (dashed lines). An initial scale factor of 1.46 was computed and applied as described in Section 2.2. The record's FAS and PSD spectra were smoothed using a Konno and Ohmachi window [31] with a bandwidth parameter b=20, consistent with the smoothing applied during the development of the target functions [32].

The ratios between the record spectra and the targets are presented in the bottom row of Figure 1. It is evident that while amplitude scaling aligns the record's response spectrum with the PSA_{target}, the stringent SRP 3.7.1 requirements are not satisfied by scaling alone.

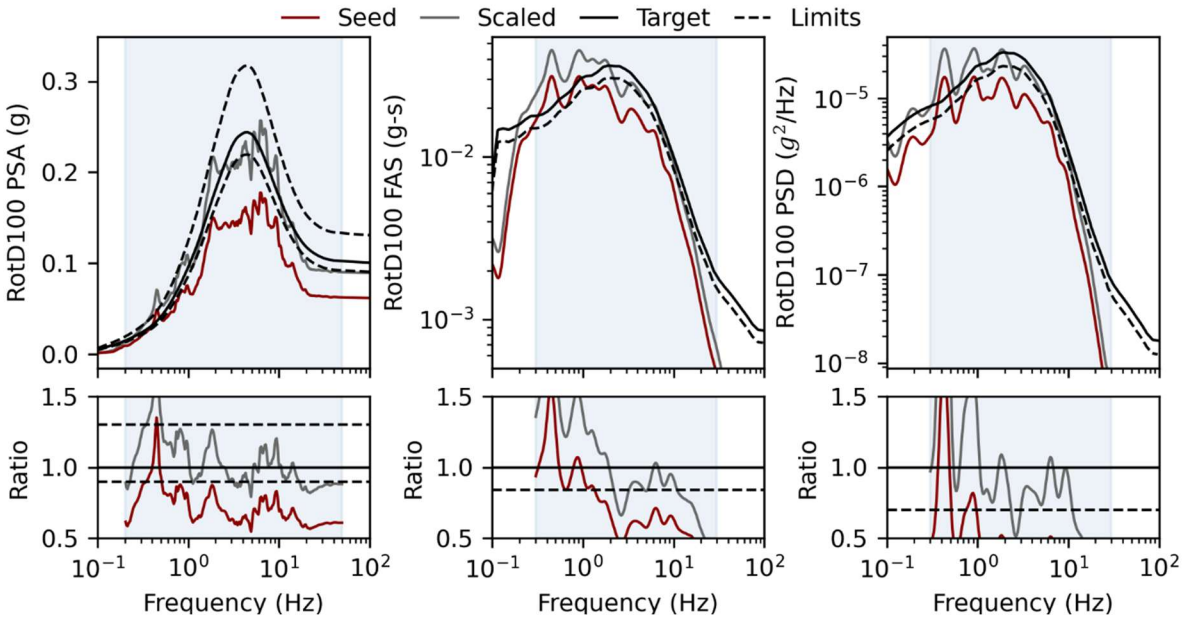

Figure 1. Top row: seed and scaled records spectra along with the target spectra and allowable limits (dashed lines). Bottom row: Ratios between the records RotD100 spectra and the target spectra.

3.3 Matching the Target Response Spectrum (Stage I)

Figure 2 presents the spectral characteristics of the record following the primary RotDnn response spectrum matching phase (Stage I). The results are denoted as 'PSA matched' and are plotted alongside the initial amplitude-scaled seed for comparison. As evidenced by the top-left panel, the CWT-based matching algorithm is highly effective: the RotD100 response spectrum of the modified record tightly conforms to the target curve across the entire frequency range of interest. The resulting spectral ratios remain strictly within the stringent 0.9 to 1.3 acceptance limits mandated by SRP 3.7.1; in fact, the limits are easily satisfied, with ratios remaining very close to unity throughout the entire frequency band.

However, an analysis of the frequency content reveals the critical limitation of relying solely on response spectral compatibility. Despite the excellent fit in the PSA domain, the record exhibits significant power deficiencies. As illustrated in the bottom row of Figure 2, the RotD100 FAS and

PSD functions fall below their respective minimum thresholds (α=0.84 and β=0.70) at several frequency bands. These excursions confirm that a record can satisfy regulatory PSA checks while failing to provide adequate energy input, validating the need for the subsequent FAS and PSD adjustment stages.

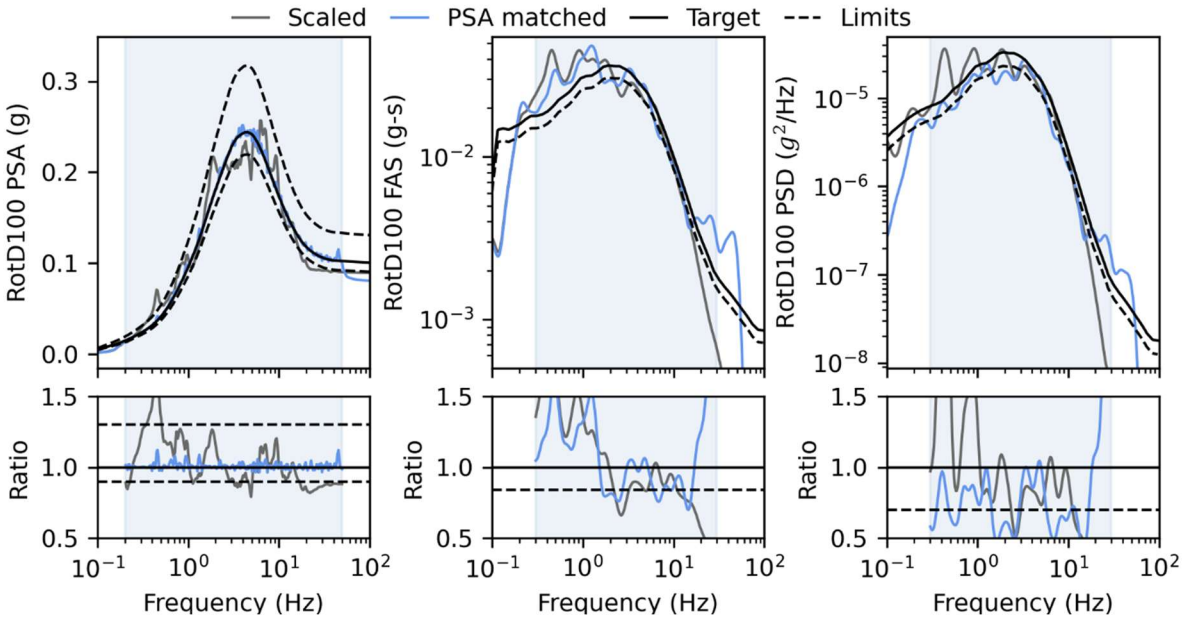

Figure 2. Top row: scaled and PSA matched records spectra along with the target spectra and allowable limits (dashed lines). Bottom row: Ratios between the records RotD100 spectra and the target spectra.

3.4 Minimum FAS Compliance (Stage II)

As identified in the previous section, the purely response-spectrum-matched record exhibits several frequency bands where the energy content falls below the acceptable threshold. To rectify this, the algorithm executes the Stage II global energy check, which is designed to enforce a minimum Fourier Amplitude Spectrum (FAS) floor.

Figure 3 illustrates the effect of this secondary adjustment. The results, denoted as ‘FAS adjusted’, demonstrate the algorithm's surgical intervention. In the middle panels (RotD100 FAS and its corresponding ratio), it is clear that the previously identified deficiencies in the "PSA matched" signal have been corrected. The iterative scaling of the critical detail functions lifts the FAS only at the frequency bands where a deficit was identified, leaving the others unaffected. Consequently, the record's FAS now strictly satisfies the minimum threshold across the entire frequency evaluation range.

Because this FAS adjustment involves a global, uniform scaling of specific time-frequency detail functions across the entire duration of the record, it inevitably perturbs the initial response spectrum match achieved in Stage I. However, as shown in the left panels of Figure 3, the narrow-band nature of the CWT decomposition ensures that this disruption is minimal. The RotD100 PSA of the FAS-adjusted record experiences slight amplifications at the targeted frequencies but remains comfortably within the stringent 0.9 to 1.3 regulatory limits.

While the FAS adjustment successfully establishes a baseline global energy floor, the right panels of Figure 3 (RotD100 PSD) reveal that global FAS compliance does not inherently guarantee PSD compliance. Although the PSD amplitudes are increased by the FAS adjustment, the record still exhibits localized dips below the 0.70 threshold. This occurs because PSD measures power (energy per unit time), and global FAS adjustments do not account for the temporal concentration of that energy, necessitating the localized Stage III PSD adjustment.

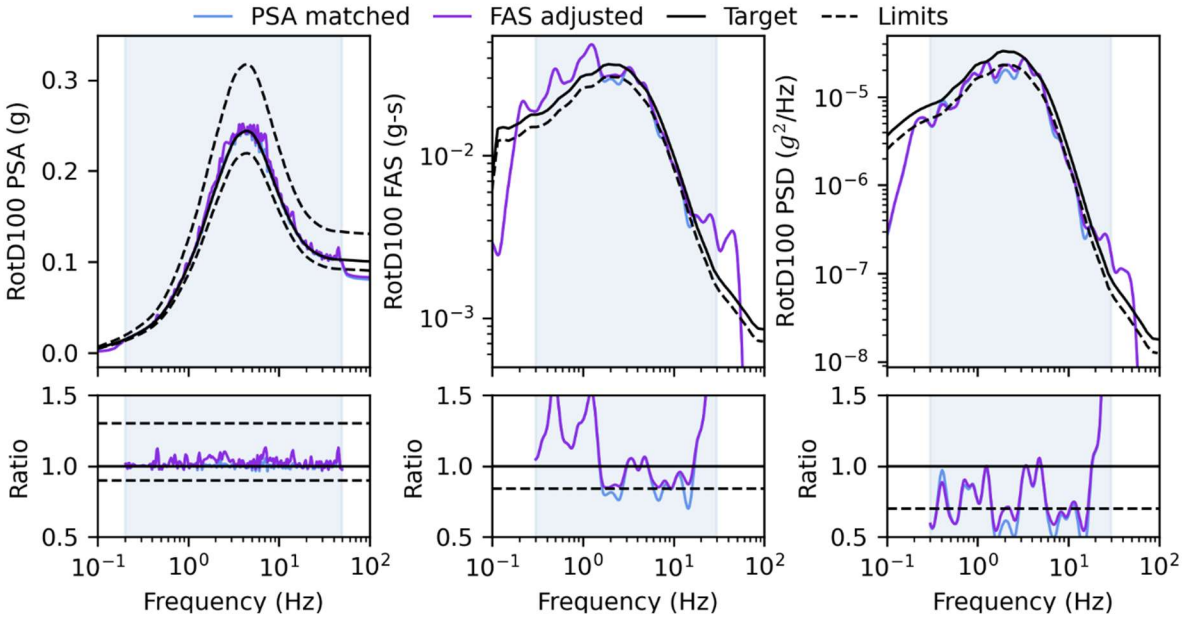

Figure 3. Top row: PSA matched and FAS adjusted records spectra along with the target spectra and allowable limits (dashed lines). Bottom row: Ratios between the records RotD100 spectra and the target spectra.

3.5 Localized RotDnn PSD Adjustment (Stage III)

To address the residual power deficiencies identified at the conclusion of Stage II, the algorithm initiates the Stage III localized PSD adjustment. As established in the methodology, attempting to rectify PSD dips by applying a global scaling factor would artificially amplify the low-energy segments of the acceleration history. Because power is a measure of energy per unit time, such a global approach risks distorting the physical realism of the ground motion and severely disrupting the response spectrum match achieved in Stage I.

Instead, Stage III employs a targeted, time-domain windowing technique. The algorithm applies corrective scaling to the deficient time-frequency detail functions exclusively within a window centered on the record's significant strong motion duration ($SD_{5\text{-}75}$).

Figure 4 presents the spectral results of this final 'PSD adjusted' record plotted against the previous iteration. The rightmost panels demonstrate the effectiveness of this targeted energy injection. Similar to the FAS modification in Stage II, the algorithm isolates and scales *only* the specific frequency bands experiencing a power deficit. As observed in the PSD plot (Figure 4, top right),

the power at the deficient frequencies is surgically lifted, while the PSD at the remaining frequencies remains almost identical to the previous iteration. Consequently, the RotD100 PSD ratio of the modified record now rests entirely above the 0.70 lower-bound threshold across the entire frequency range of interest, successfully eliminating the localized dips that persisted after the FAS adjustment.

The left and middle panels of Figure 4 confirm the robustness of utilizing localized CWT modifications. By concentrating the added energy strictly within the pre-existing strong motion envelope, the peak structural response is minimally perturbed. The final RotD100 PSA remains highly stable and strictly maintains its tight match to the target spectrum, comfortably satisfying the 0.9 to 1.3 regulatory limits set forth in SRP 3.7.1. The final algorithm thereby produces a unified record pair that simultaneously satisfies the stringent requirements for peak response (PSA), global energy (FAS), and localized power density (PSD).

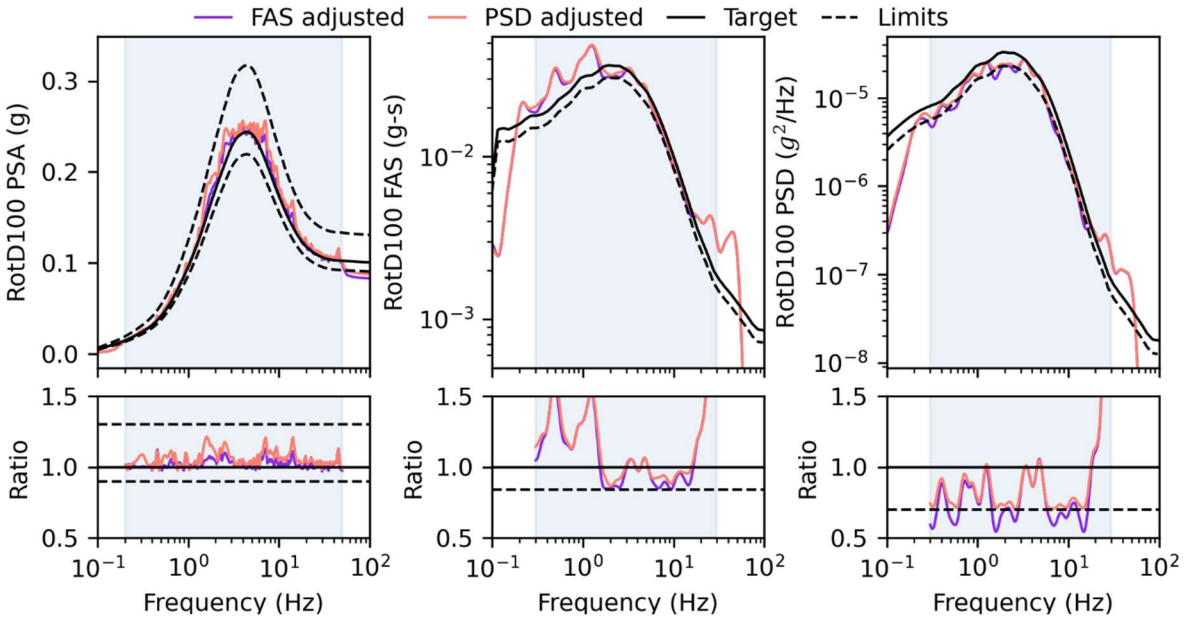

Figure 4. Top row: FAS adjusted and PSD adjusted records spectra along with the target spectra and allowable limits (dashed lines). Bottom row: Ratios between the records RotD100 spectra and the target spectra.

3.6 Preservation of Time-Domain and Directional Characteristics

A primary critique of traditional spectral matching techniques is their tendency to severely distort the physical realism of the seed ground motion, artificially inflating the number of strong motion cycles or scrambling the natural polarization of the seismic waves. A central objective of the proposed CWT-based methodology is to satisfy stringent frequency-domain energy requirements while reasonably preserving the time-domain non-stationarity and spatial directionality of the original record.

Figure 5 demonstrates the general preservation of the time-domain characteristics across all three adjustment stages for the selected record. The figure plots the acceleration, velocity, and

displacement time histories for both horizontal components, alongside their respective normalized cumulative squared values (CSA, CSV, and CSD). Despite undergoing rigorous modifications for PSA, FAS, and PSD compliance, the modified record generally retains the non-stationary amplitude envelope of the scaled seed. The normalized cumulative energy curves, which track the accumulation of energy over time, show a high degree of similarity across all iterations.

To quantify the changes in the energy build-up introduced by spectral matching, the maximum absolute differences in the normalized cumulative curves ($max\ \Delta$) were evaluated. Grant and Diaferia [33] proposed conservative upper bounds for these differences to avoid introducing unconservative bias in structural analyses, suggesting limits of 0.20 for the maximum normalized difference in Arias Intensity (equivalent to CSA) and CSV, and 0.40 for CSD. As observed in Figure 5, the $max\ \Delta$ values for the modified record remain well below these thresholds (e.g., reaching maximums of 0.07 for acceleration, 0.05 for velocity, and 0.14 for displacement). This confirms that the localized, time-windowed injections applied during Stage III effectively prevented the artificial lengthening of the strong motion duration without excessively manipulating the temporal accumulation of energy. Furthermore, the overall stability of the displacement time histories indicates that the low-frequency characteristics of the seed record were not severely corrupted by the matching process.

In addition to time-domain fidelity, the algorithm is specifically designed to largely preserve the multidirectional properties of the ground motion. Because the proposed CWT-based algorithm applies the same frequency-dependent scaling factor simultaneously to the detail functions of both orthogonal components, the relative amplitude and phase relationships between the components are maintained.

Figure 6 visually confirms this by presenting polar plots of the normalized spectral acceleration versus orientation angle at selected frequencies (from 1 Hz to 20 Hz) for the evaluated record. The characteristic "peanut" shapes, which dictate the principal directions of shaking at specific frequencies, exhibit a strong resemblance to those of the original seed record across the PSA, FAS, and PSD adjustment stages.

This preservation of natural polarization is further quantified in Figure 7, which evaluates earthquake directionality using two different metrics: the frequency-dependent RotD100/RotD50 ratios (left panel) and a directionality factor (DF) spectrum (right panel). The DF is defined as the square root of the ratio of the area of a circle circumscribing the maximum response to the area enveloping the actual response across all angles [23]. As shown in the figure, both the matched and adjusted signals closely track the complex, highly variable directionality profiles of the original seed across the frequency spectrum. This confirms that the proposed multi-stage matching algorithm can successfully upgrade the seed record's energy content to meet regulatory safety thresholds without severely sacrificing its fundamental seismological footprint or introducing artificial directional bias.

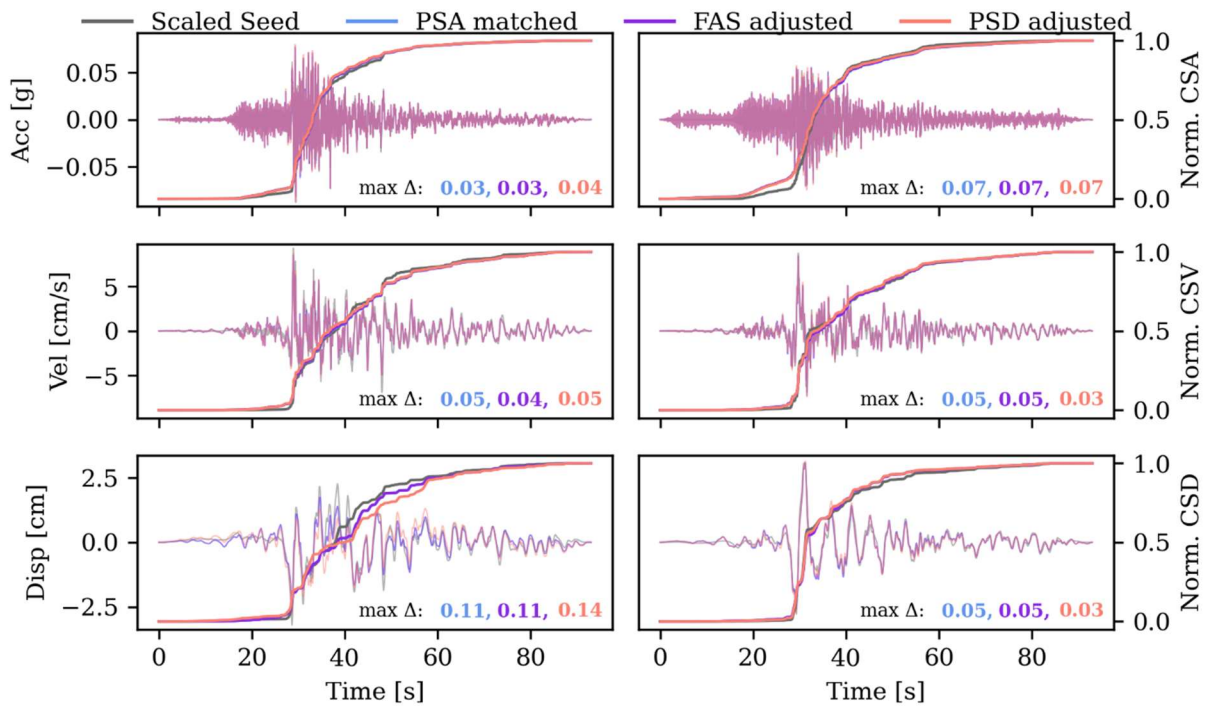

Figure 5. Each column corresponds to a horizontal component. Top row: time histories of acceleration and normalized cumulative squared acceleration (CSA). Middle row: time histories of velocity and normalized cumulative squared velocity (CSV). Bottom row: time histories of displacement and normalized cumulative squared displacement.

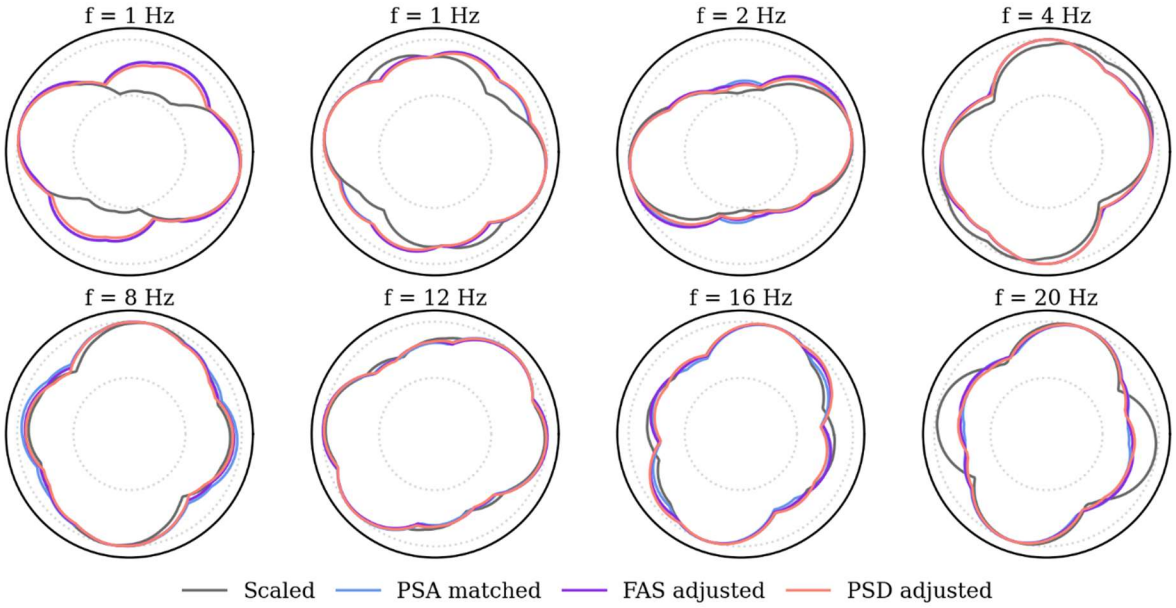

Figure 6. Normalized spectral acceleration versus orientation angle at selected periods for the scaled, PSA matched, FAS adjusted and PSD adjusted records.

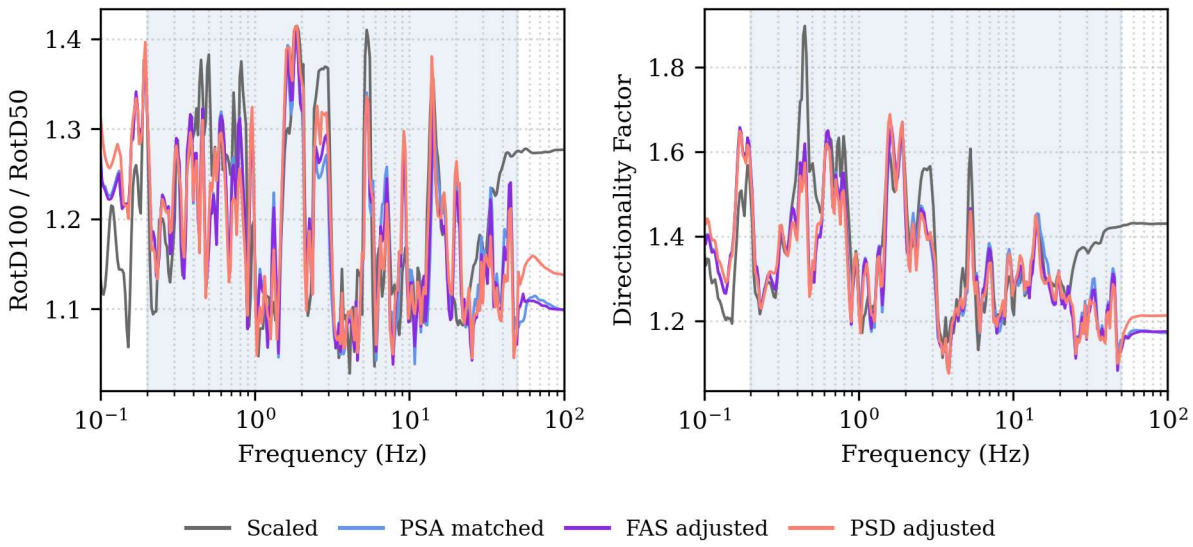

Figure 7. PSA RotD100/RotD50 ratios (left) and PSA directionality response spectra for the scaled, PSA matched, FAS adjusted and PSD adjusted records.

4. Performance Evaluation and Seed Record Selection

To rigorously evaluate the performance of the proposed multi-stage matching algorithm and establish robust criteria for seed record selection, a comprehensive numerical study was conducted using 313 bidirectional ground motion records. Seed records were sourced from the NGA-West2 database, with selection prioritized based on the initial pseudo-spectral acceleration (PSA) shape's alignment with the target RotD100 spectrum.

4.1 Multi-Stage Matching Performance

The target scenario for this evaluation is identical to the one established in Section 3: a M_w7 event at R_{JB} 50km with a target strong motion duration $SD_{5\text{-}75}$ of 10.4 seconds. Figure 8 displays the RotD100 PSA, FAS, and PSD spectra of the 313 seed records after the initial amplitude scaling stage, alongside the suite's mean and the regulatory limits. As a set, the mean of the amplitude scaled records successfully approximates the target PSA while complying with the regulatory limits; however, it fails to satisfy the minimum PSD bounds, falling significantly short at frequencies above approximately 10 Hz.

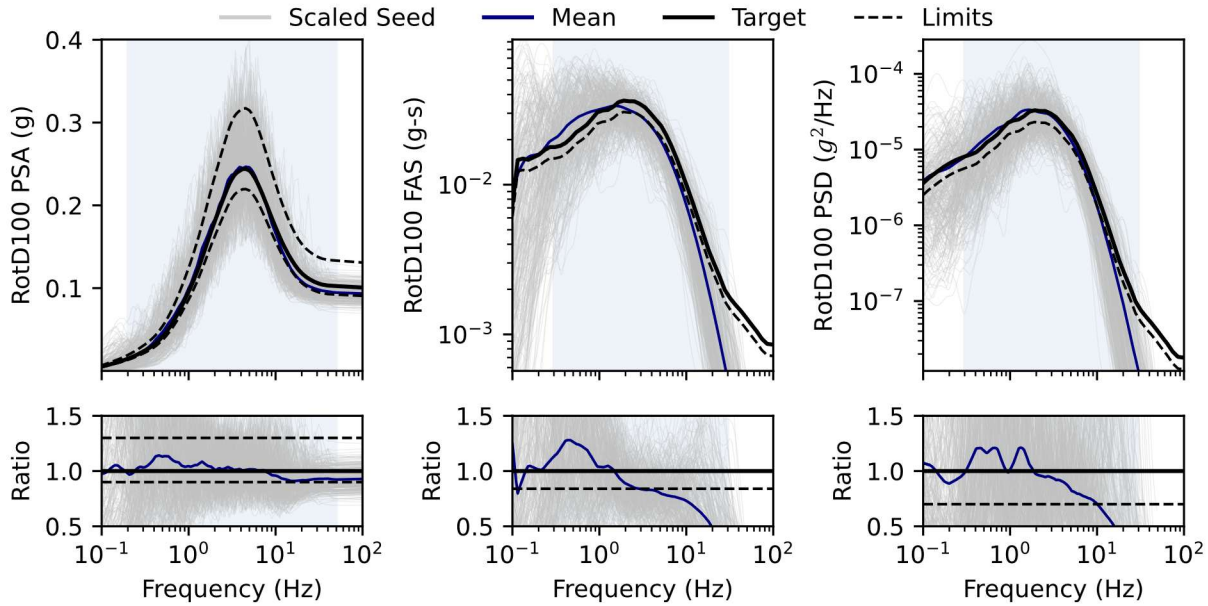

Figure 8. Spectra from the 313 seed records after initial amplitude scaling (gray lines) and the set mean (blue line), alongside the target RotD100 spectra and allowable limits (dashed lines). Bottom row: Ratios between the individual records' RotD100 spectra and the targets.

The records were subsequently processed through the complete proposed algorithm, including Stage I (PSA matching), Stage II (FAS adjustment), and Stage III (Localized PSD adjustment). Figure 9 presents the final adjusted spectra. The algorithm successfully lifts the suite's mean entirely above the 0.84 FAS and 0.70 PSD minimum energy thresholds while still maintaining strict compliance with the target RotD100 PSA limits. Thus, as a set, the matched suite fully complies with all three spectral requirements. However, an examination of the individual record traces (gray lines) reveals that while the mean is compliant, many individual records heavily diverge and fail to meet the stringent criteria on their own.

Figure 10 examines the preservation of ground motion directionality by comparing the RotD100/RotD50 ratios of the 313 seed records against the final PSD-adjusted records across the PSA, FAS, and PSD domains. As observed, the proposed matching algorithm preserves the inherent multi-directional characteristics of the original seed motions. The FAS RotD100/RotD50 ratio of the matched records remains highly stable across the entire frequency spectrum at approximately 4/3, corroborating recent findings on the properties of orientation-independent Fourier spectra [32]. In contrast, the PSA ratio exhibits its characteristic and well-documented frequency-dependent behavior, which is also faithfully tracked by the modified records. For the PSD, the square root of the ratio is presented to maintain a comparable scale, showing similarly strong preservation. The closely overlapping means and ±1 logarithmic standard deviation bounds (shaded regions) confirm that the adjustments applied do not introduce artificial directional bias or distort the fundamental statistical relationship between the maximum and median horizontal spectral amplitudes.

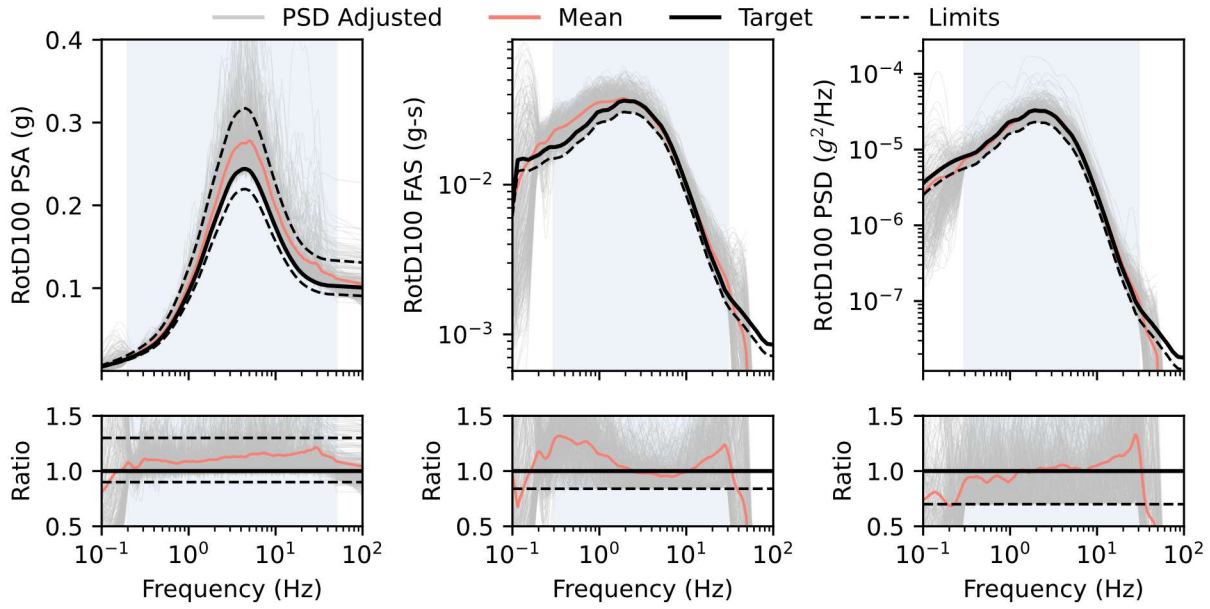

Figure 9. Spectra from the 313 records after the final multi-stage matching process (PSD adjustment). The set mean (blue line) demonstrates simultaneous compliance across all three spectral domains.

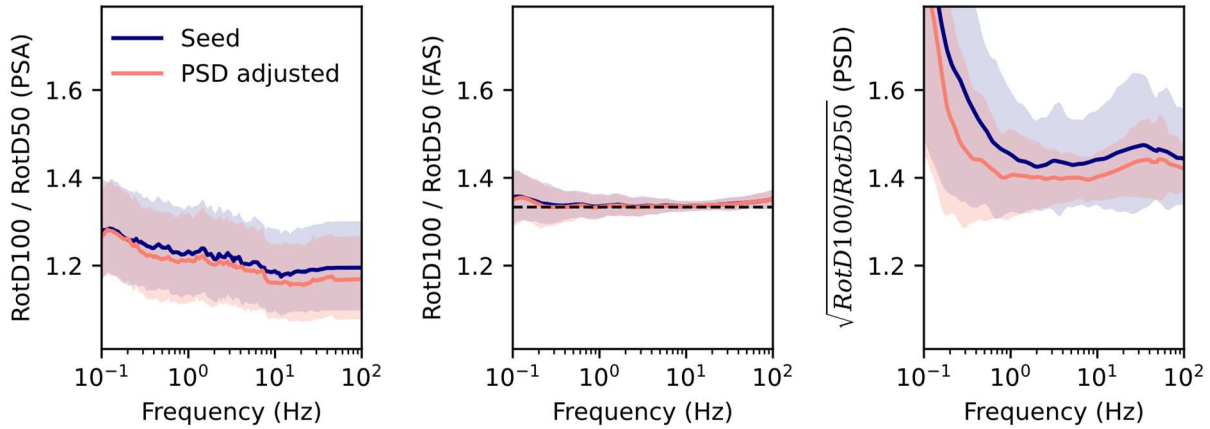

Figure 10. Mean RotD100/RotD50 ratios for PSA (left) and FAS (center), and the square root of the RotD100/RotD50 ratio for PSD (right) for the 313 seed records and the final Stage III (PSD adjusted) records. The shaded regions denote the mean ± 1 logarithmic standard deviation bounds. The dashed horizontal line in the center panel represents the 4/3 reference ratio for FAS [32].

4.2 Failure Modalities and the 1.3 PSA Limit

According to the US-NRC Standard Review Plan (SRP) 3.7.1, the criteria for enveloping the design response spectra and maintaining sufficient power over the frequency range of interest are ultimately applied to the average of a multiple time-history suite. Therefore, the fact that an individual record is not in full compliance does not inherently require it to be discarded; in

conjunction with the other records, the set's mean may still comply, especially if the individual deviations are small.

Nevertheless, evaluating the strict compliance of individual records provides critical insight into the algorithm's limitations and the physical constraints of spectral matching. An individual match was deemed a "failure" if it violated the PSA bounds [0.9 - 1.3], the FAS minimum [>0.84], or the PSD minimum [>0.70]. Furthermore, self-imposed conservative criteria were placed on the time-domain energy accumulation ($\Delta CSA \leq 0.20$, $\Delta CSV \leq 0.20$, $\Delta CSD \leq 0.40$). These maximum Δ bounds were established to satisfy the SRP 3.7.1 mandate that the "phasing characteristics of the earthquake records should not change significantly" during the matching process. When evaluated against these strict individual constraints, only 29 out of the 313 records (approximately 10%) achieved full compliance across all criteria.

Figure 11 visualizes the failure signatures for the evaluated dataset. The left plot presents a failure heatmap, mapping each of the 313 records (sorted descending by their final maximum PSA ratio) against the discrete failure criteria, where pink indicates a failure (non-compliance) and blue indicates a pass (compliance). This visual matrix demonstrates the overlapping nature of the failures, revealing that records suffering from massive PSA overshoots also frequently trigger the time-domain Δ flags and residual FAS/PSD deficiencies. The Pareto chart on the right quantifies this, revealing that exceeding the maximum PSA limit of 1.3 is the overwhelmingly dominant failure mode, present in almost 85% of all non-compliant records (either alone or in combination with other failures). Algorithmically, this occurs because if, after Stage I (PSA spectral matching), the record still exhibits deep spectral energy "holes," the algorithm must significantly increase the contribution of the wavelet detail functions corresponding to the deficient frequencies to pull the signal above the minimum thresholds. This massive energy injection inevitably disrupts the time series and artificially inflates the peak response beyond the 1.3 ceiling.

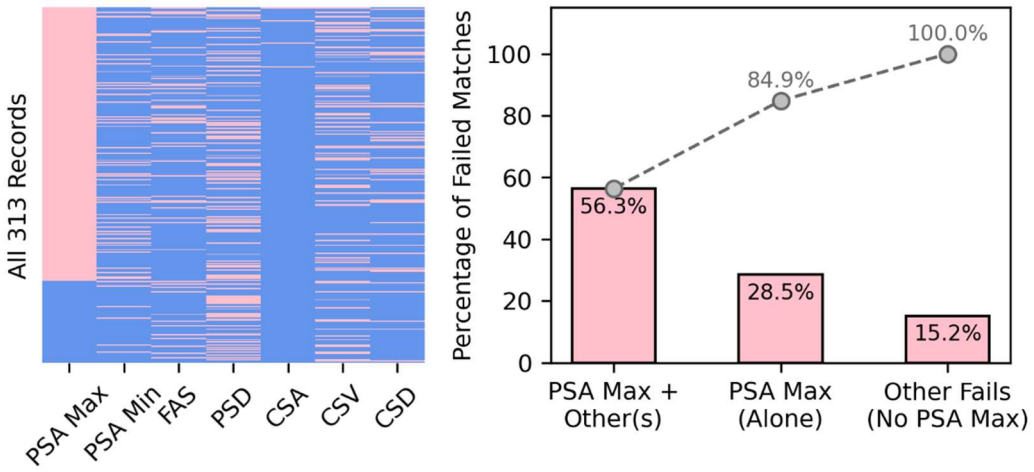

Figure 11. Left: Failure signature heatmap for all 313 records, sorting the discrete failure flags for each record by its maximum PSA ratio (pink denotes failure, blue denotes compliance). Right: Pareto chart illustrating the distribution of failure categories, highlighting the dominance of the PSA upper limit exceedance.

4.3 Identifying Drivers of Noncompliance and Screening Criteria

While the previous sections demonstrated that multi-domain compliance is difficult to achieve, the objective is to systematically identify the initial seed parameters that drive eventual matching success and establish actionable screening guidelines.

4.3.1 Definition of Predictor Variables

Before conducting the statistical and algorithmic evaluations, a comprehensive set of predictor variables (features) was extracted from the 313 initially scaled seed records. These parameters quantify the initial amplitude, spectral shape, global energy, and duration compatibility of the seeds relative to the target scenario. The full statistical distribution of these parameters across the database is summarized in Table 1.

- *Scale Factor:* The linear amplitude multiplier applied to the raw seed to minimize initial response spectral misfit.
- *PSA RMSRE:* The Root Mean Squared Relative Error between the scaled seed's PSA and the target PSA. Utilizing RMSRE normalizes the error at each frequency point relative to the target amplitude, ensuring a balanced evaluation of spectral shape conformity. Notice that the seeds were pre-screened for visual shape compatibility, so the variability of this parameter is less than the expected from randomly selected records.
- *SD5-75 AbsRel Diff:* The absolute relative difference (percentage magnitude) between the seed's significant strong motion duration and the target scenario's duration.
- *SD5-75 Rel Diff:* The directional relative difference between the seed and target durations (a negative value indicates the seed is shorter).
- *FAS & PSD MeanAbsLog:* The mean of the absolute logarithmic differences between the seed's spectra (FAS and PSD) and the target spectra over the evaluation frequency range, quantifying the overall global energy deficit.
- *FAS & PSD MaxNegLog:* The maximum negative logarithmic difference between the seed's spectra and the targets, identifying the single deepest spectral gap or energy "hole" in the initial record.

Table 1. Statistical distribution of the initial predictor variables across the 313 pre-screened seed records.

	Mean	*Std. Dev.*	*Min.*	*25th Perc.*	*Median*	*75th Perc.*	*Max.*
Scale Factor	1.681	1.35	0.17	0.657	1.304	2.23	6.266
PSA RMSRE	0.32	0.12	0.138	0.235	0.291	0.375	0.993
SD5-75 AbsRel Diff	0.372	0.319	0	0.155	0.31	0.491	1.884
SD5-75 Rel Diff	0.038	0.489	-0.861	-0.311	-0.061	0.296	1.884
FAS MeanAbsLog	0.202	0.072	0.064	0.149	0.195	0.249	0.478
FAS MaxNegLog	0.758	0.341	0.073	0.51	0.732	0.955	1.942
PSD MeanAbsLog	0.381	0.129	0.133	0.281	0.365	0.472	0.932
PSD MaxNegLog	1.529	0.643	0.291	1.012	1.48	2.008	3.24

4.3.2 Correlation Analysis

To identify the independent baseline drivers of eventual noncompliance, a Spearman correlation analysis was performed comparing the initial parameters against the final Maximum PSA Ratio achieved after adjustment. Because exceeding the 1.3 upper tolerance limit was previously identified as the overwhelmingly dominant failure mode, the peak PSA ratio serves as a highly sensitive, continuous proxy for overall matching severity. The resulting matrix is presented in Figure 12. Several critical implications arise from these correlations:

- Initial PSA fit: The correlation between the initial *PSA RMSRE* and the final *Maximum PSA Ratio* is remarkably low (0.05). This illustrates a classic statistical "restriction of range" effect. As mentioned earlier, the 313 records were originally pre-screened to possess a reasonable baseline resemblance to the target PSA, the variances remaining in their initial PSA fits may hold limited predictive power.
- Initial FAS and PSD fits (Energy Content): While all four metrics measuring energy content (*FAS MeanAbsLog*, *FAS MaxNegLog*, *PSD MeanAbsLog*, and *PSD MaxNegLog*) are highly inter-correlated with each other (exhibiting correlation coefficients ranging from 0.57 to 0.91), the initial Fourier amplitude misfit (*FAS MeanAbsLog*) stands out as the strongest individual predictor not only from the energy related metrics but from all 9 parameters investigated with a correlation factor of 0.39. Physically, this aligns with the observation that seeds harboring massive hidden energy deficits require aggressive, localized manipulations during Stages II and III, thereby overshooting the previously matched PSA.
- Scenario strong motion duration compatibility: The parameter with the second-largest correlation to the final *Maximum PSA Ratio* is the absolute relative duration difference (*SD5-75 AbsRel Diff*, 0.33). This finding corroborates previous research which identified that selecting seed records with an initial significant duration close to the target scenario is a critical factor for multi-domain matching success [34]. Moreover, the directional duration difference (*SD5-75 Rel Diff*) showed limited correlation (-0.08), indicating that the magnitude of the duration mismatch drives failure, regardless of whether the initial record is too short or too long.

- Scale Factor: Historically, the use of large scale factors has been penalized under the assumption that large amplitude multipliers produce unrealistic records. However, the correlation analysis yielded a coefficient of -0.13, indicating that the initial amplitude scale factor has a negligible effect on final record compliance.

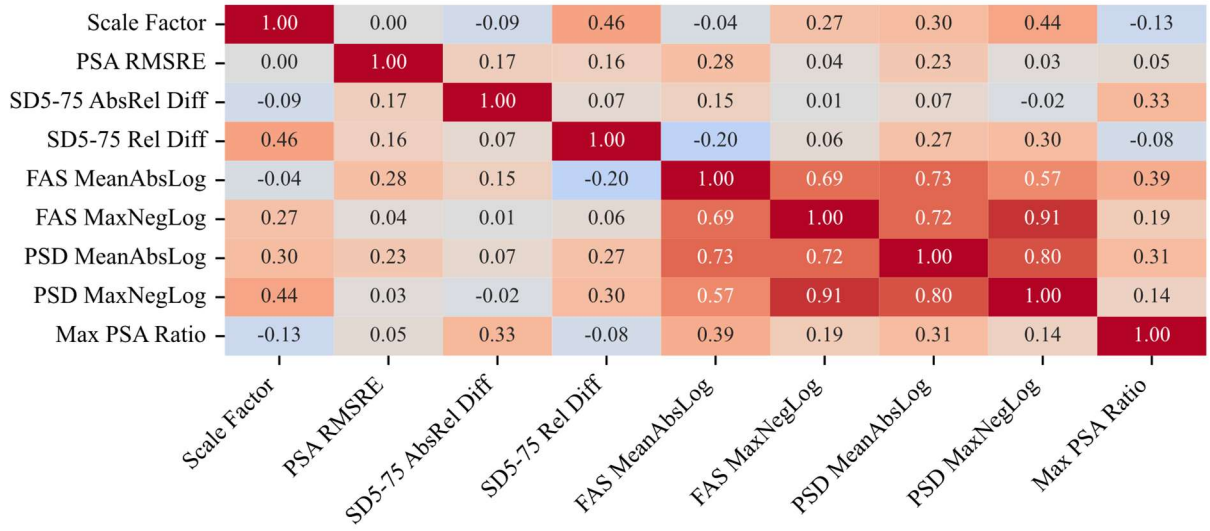

Figure 12. Spearman correlation matrix

4.3.3 Decision Trees and The Limitation of a Single Global Filter

While the correlation matrix identifies broad, independent data trends, machine learning algorithms are required to mathematically isolate the specific combinations of seed characteristics that guarantee successful multi-domain matches. Decision tree algorithms are particularly ideal for this task. Unlike traditional multivariate regression models that assume linear, proportional relationships across the entire dataset, decision trees naturally produce hierarchical, non-linear, and easily interpretable threshold boundaries.

Initially, a global Binary Classification Tree was trained on the entire dataset to predict full compliance across all seven frequency and time-domain criteria simultaneously. However, because the vast majority of randomly selected seeds fail at least one strict constraint, the dataset is heavily skewed. When forced to apply a single pass/fail filter, the algorithm became trapped by this class imbalance, overwhelmingly predicting failure across almost all branches and failing to capture a generalized screening rule. This demonstrated that multi-domain compliance cannot be efficiently achieved through a single, blunt filter. Instead, a two-tiered approach is required: first filtering for frequency-domain stability (PSA, FAS, and PSD related criteria) and then isolating for time-domain fidelity (ΔCSD, ΔCSV, and ΔCSD criteria).

4.3.4 Tier 1: Regulatory Spectral Energy Compliance

Because exceeding the 1.3 upper PSA limit is the dominant failure mode, a Regression Decision Tree was trained to predict the final *Maximum PSA Ratio* based on the initial predictor variables. A regression approach, rather than binary classification, is ideal for this primary stage because

regulatory requirements (PSA and PSD) are ultimately verified against the suite mean, not individual records. Therefore, individual records slightly exceeding these limits should not be immediately discarded, as compliance can still be achieved when their spectra are averaged within a suite.

As seen in Figure 13, this algorithm successfully identified the safe pathways that prevent massive spectral overshoots. To achieve a high probability of suite-averaged regulatory frequency compliance, seed records must satisfy the following Tier 1 criteria:

1. *FAS MeanAbsLog* $\leq$ *0.302*: *FAS MeanAbsLog* emerges as the primary splitting node, superseding the initial spectral fit (*PSA RMSRE*). This perfectly aligns with the correlation analysis (Figure 11); because the remaining differences in PSA fit of the selected record hold limited predictive power, the hidden global energy deficits (measured through FAS) become the dominant forcing function for algorithmic overshoots.
2. *PSA RMSRE* $\leq$ *0.762*: The initial spectral shape must reasonably approximate the target.
3. *SD5-75 AbsRel Diff* $\leq$ *0.330*: The seed's significant duration must be within 33% of the target scenario's duration.

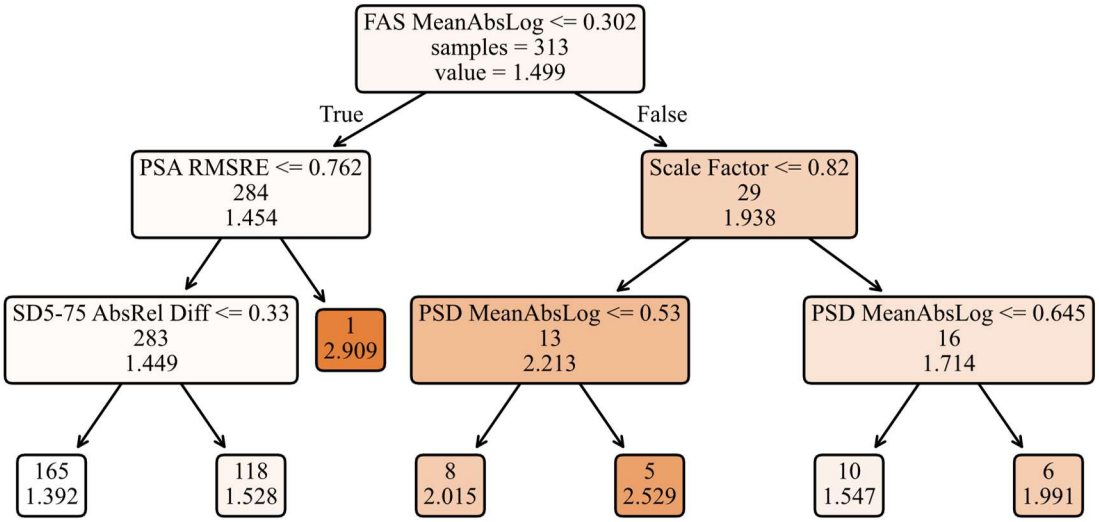

Figure 13. Tier 1 Decision Tree Regressor

When applied to the database, 166 records successfully passed this screen. A Monte Carlo simulation was performed to statistically validate these criteria. Different set sizes were evaluated: 3, 5, 7, 9, and 11 records. For each size, 100,000 sets were randomly constructed, and the criteria were checked against the sets' means. The results are presented in Figure 14, the bars represent the success rate for each of the 4 frequency domain criteria. It is seen that when evaluating exclusively for frequency-domain regulatory criteria (the black line), the Tier 1 parameters perform exceptionally well: for a standard 7-record suite, the expected success rate is 97.2%. As expected, the larger the set, the larger the likelihood of their means being in compliance. Moreover, notice

that Max PSA Ratio was the criteria controlling all cases, with the other frequency domain criteria at 100% compliance.

Nevertheless, when the auto-imposed time-domain fidelity constraints are enforced (Total Compliance, red line), the success rate drops dramatically, falling to 11.5% for a 7-record suite. Because these physical preservation constraints are evaluated on an individual-record basis, a single failing record corrupts the entire suite, strictly limiting the effectiveness of the Tier 1 filter alone.

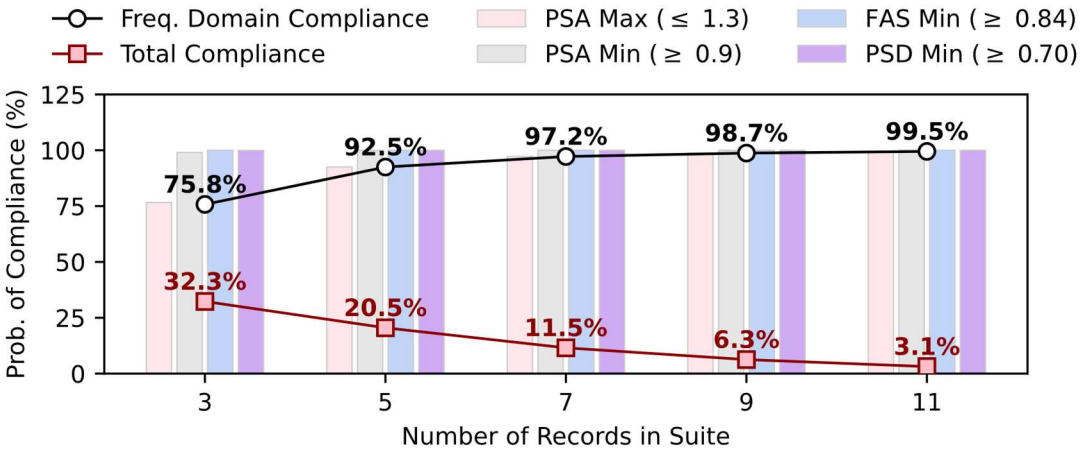

Figure 14. Compliance Monte Carlo sim tier 1

4.3.5 Tier 2: High-Fidelity Signal Preservation

To address the time-domain distortion, a secondary Binary Classification Tree (Figure 15) was applied exclusively to the subset of 165 records that successfully passed the Tier 1 screen.

The tree mathematically proved that to increase the likelihood of preserving time-domain characteristics (preventing ΔCSA, ΔCSV, and ΔCSD limits from being exceeded), the matching algorithm's intervention must be minimized by further tightening the initial tolerance bounds. Synthesizing the limits from this secondary tree with the Tier 1 boundaries yields a subset of high-fidelity seeds:

1. *-31.9% ≤ SD5-75 Rel Diff ≤ +33.0%*: The tree demonstrates that records missing more than 32% of the target duration lack the necessary physical wave cycles to absorb spectral corrections naturally, guaranteeing velocity drift.
2. *PSA RMSRE ≤ 0.251*: Tightened initial response spectra fit limit
3. *FAS MeanAbsLog ≤ 0.254*: Tightened initial FAS fit limit.

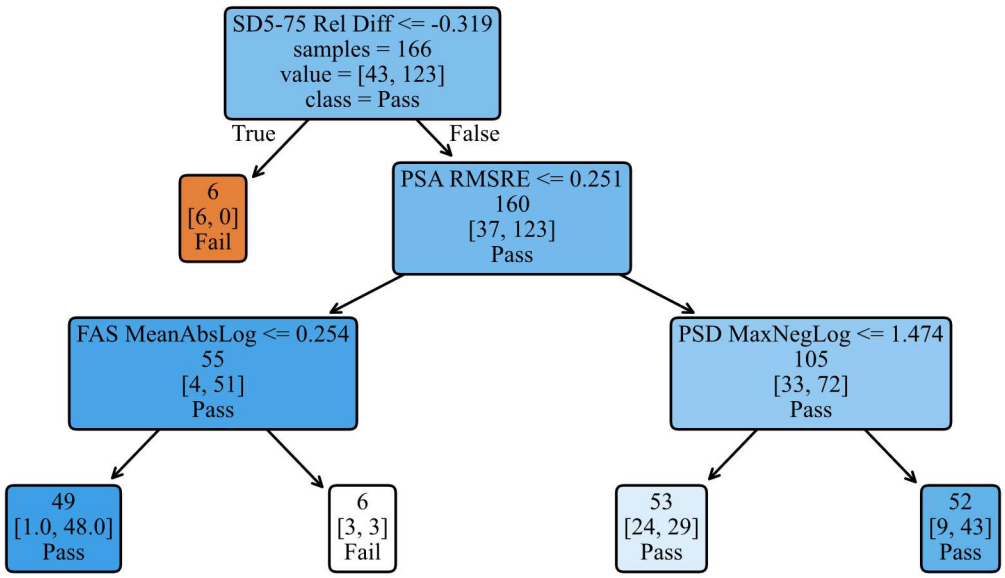

Figure 15. Tier 2 Binary Decision Tree

Applying these stricter constraints isolated a subset of 48 motions, the results from a Monte Carlo simulation using this subset are presented in Figure 16. For the sake of clarity this figure only presents individual results (bars) for the time domain criteria. However, the compliance rate indicated in the text annotations accounts for all 7 criteria. It is seen that under these stringent conditions, ΔCSA and ΔCSV drift are entirely eliminated. The overall set compliance percentage is governed by the ΔCSD limit for all suite sizes, except for the 3-record suites, where it is controlled by a combination of the Maximum PSA Ratio and ΔCSD. In general, the likelihood of total multi-domain compliance is significantly increased, for example, a 7-record suite surges from 11.5% to 85.1%.

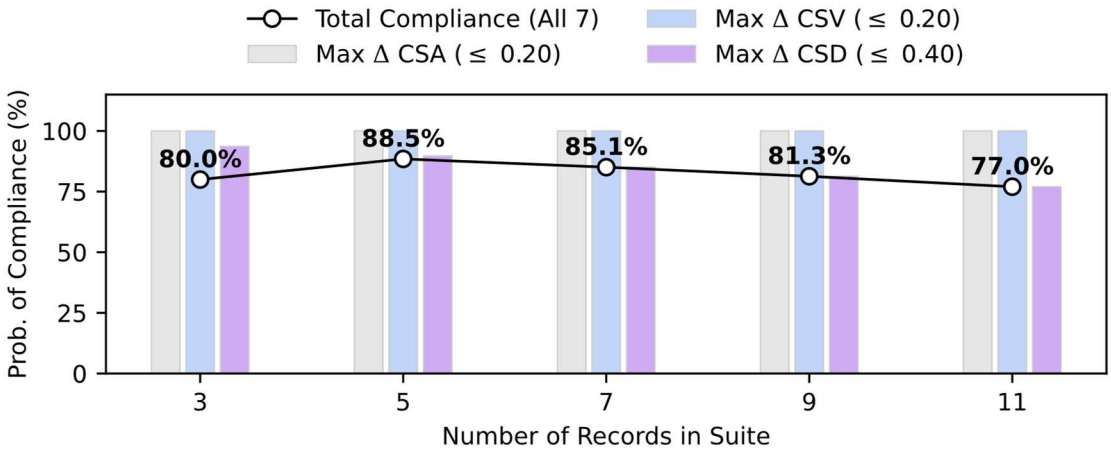

Figure 16. Compliance Monte Carlo sim tier 2

5. Conclusions

The seismic assessment of critical infrastructure increasingly demands acceleration time histories that tightly match a target response spectrum without inadvertently depleting the signal's fundamental energy content. This study presented a unified, Continuous Wavelet Transform (CWT)-based spectral matching algorithm capable of simultaneously satisfying stringent orientation-independent (RotD100) response spectra tolerances, minimum global Fourier Amplitude Spectrum (FAS) floors, and localized Power Spectral Density (PSD) requirements. By systematically integrating global frequency adjustments with the localized scaling of time-frequency detail functions, the proposed methodology resolves the energy-deficiency vulnerabilities inherent in traditional spectral matching, ensuring robust compliance with strict regulatory frameworks such as US-NRC SRP 3.7.1.

At the individual record level, the algorithm successfully circumvents the primary critiques of traditional spectral matching. Because the CWT framework modifies the intensity of existing energy packets rather than superimposing artificial wavelets, it was shown to preserve the non-stationary temporal envelope of the seed motion. Furthermore, by applying consistent scaling factors to the detail functions of both orthogonal components simultaneously, the algorithm accurately maintains the natural multidirectional polarization and directionality profiles of the original seismic wave.

To rigorously evaluate the algorithm's multi-domain matching performance and establish actionable guidelines for practitioners, a comprehensive statistical evaluation was conducted on 313 bidirectional ground motion records. Monte Carlo simulations spanning various suite sizes (3, 5, 7, 9, and 11 records) revealed that while achieving simultaneous multi-domain compliance is inherently difficult, mathematical boundaries can be established to systematically increase the probability of success. For instance, while initial (Tier 1) frequency-domain screening yielded a 97.2% frequency compliance rate for a 7-record suite, the total multi-domain compliance rate remained low (11.5%) due to time-domain deviations. However, when suites were assembled from seed motions meeting strictly defined, machine-learning-derived initial criteria (Tier 2 constraints), artificial acceleration and velocity deviations were eliminated, and the probability of total multi-domain compliance for a 7-record suite surged to 85.1%.

The following critical insights and practical guidelines emerged from the statistical evaluation of the matching process:

- The role of global energy in pre-screened seeds: While an initial visual resemblance to the target spectral shape (*PSA RMSRE*) remains a fundamental prerequisite for seed selection (and is maintained as a required boundary in the decision trees), its variability within the pre-screened database was restricted. Consequently, for records that already possess a reasonable initial PSA fit, spectral energy mismatch—measured via the *FAS MeanAbsLog*—emerges as the dominant predictor of algorithm failure. Seeds harboring large energy deficits require aggressive detail functions scaling that inevitably over-amplifies the peak response, driving the final maximum PSA ratio beyond the 1.3 regulatory ceiling.

- FAS as a screening proxy: The correlation analysis demonstrated that *FAS MeanAbsLog* is highly inter-correlated with all other energy metrics, including those based on PSD. This finding is highly advantageous for practitioners. The computation of orientation independent RotDnn PSD is more mathematically sensitive (e.g. defining the portion of the signal than can be assumed stationary remains debatable) and computationally expensive (need to be computed for each direction) than FAS. Moreover, while ground motion models exist and are continually being developed for FAS, they remain scarce for PSD. Most important, modern databases, such as the New Zealand Ground-Motion Database [35] and the upcoming NGA-West3 [36], have started incorporating FAS data directly into their flatfiles - allowing practitioners to use this accessible metric to screen seed records for multi-domain energy compliance.
- Time-domain limits and SRP 3.7.1 phasing requirements: The strict time-domain preservation criteria imposed in this study (ΔCSA, ΔCSV, and ΔCSD) were utilized as measurable constraints to satisfy the SRP 3.7.1 mandate that the phasing characteristics of the seed records must not change significantly. These cumulative metrics relate to the dynamic response of different structural types depending on the relevant frequency bands. For instance, CSA is typically associated with high-frequency radiated power. This makes it a relevant parameter for relatively rigid structural systems responding predominantly in the linear elastic range—such as nuclear power facilities and heavy industrial containments. Conversely, CSV reflects the transfer of kinetic energy and the potential presence of intermediate-frequency velocity pulses. This parameter tends to influence peak interstory drift in more flexible systems, such as regular civil structures explicitly detailed to endure significant inelastic excursions. Finally, CSD is generally associated with low-frequency energy and baseline drift. While the Tier 2 screening in this study successfully minimized acceleration and velocity drift, most of the remaining noncompliance cases were governed by ΔCSD. Because the low-frequency energy tracked by the CSD typically has a lesser impact on standard interstory drift and high-frequency ISRS demands compared to CSA and CSV, the exceedances in ΔCSD might be considered acceptable following a visual inspection of the displacement time histories. This suggests that the practical success rate of the algorithm may be somewhat higher than the strict mathematical values reported.

Ultimately, this study demonstrates that by pairing the proposed multi-stage CWT algorithm with the algorithmically derived Tier 2 screening boundaries, practitioners can reliably generate high-fidelity, multidirectional ground motions that satisfy the industry's most rigorous seismic requirements. Note that the practical implementation of this methodology is highly streamlined; every metric utilized in these screening recommendations—including initial spectral shape compatibility, significant strong motion duration, and global spectral energy misfit (via FAS)—can be directly extracted or efficiently computed from the standard metadata readily available in modern earthquake database flatfiles.

Data and Resources

A Python implementation of the proposed algorithm is available from the author GitHub repository.

Acknowledgements

This research was performed under award number 31310024M0015 from the US Nuclear Regulatory Commission. The statements, findings, conclusions, and recommendations are those of the author and do not necessarily reflect the view of the US Nuclear Regulatory Commission.

References

[1] USNRC, 2014, "Section 3.7.1., Seismic Design Parameters, Revision 4. NUREG0800 Standard Review Plan."
[2] American Society of Civil Engineers, 2017, *Seismic Analysis of Safety-Related Nuclear Structures*, American Society of Civil Engineers, Reston, VA. https://doi.org/10.1061/9780784413937.
[3] Gascot, R. L., and Montejo, L. A., 2016, "Spectrum-Compatible Earthquake Records and Their Influence on the Seismic Response of Reinforced Concrete Structures," Earthq. Spectra, **32**(1), pp. 101–123. https://doi.org/10.1193/011714EQS010M.
[4] Kaul, M. K., 1978, "Spectrum-Consistent Time-History Generation," J. Eng. Mech. Div., **104**(4), pp. 781–788. https://doi.org/10.1061/JMCEA3.0002379.
[5] Lilhanand, K., and Tseng, W. S., 1987, "Generation of Synthetic Time Histories Compatible with Multiple-Damping Design Response Spectra," *Transactions of the 9th International Conference on Structural Mechanics in Reactor Technology*, Lausanne.
[6] Abrahamson, N. A., 1992, "Non-Stationary Spectral Matching," Seismol. Res. Lett., **63**(1), p. 30.
[7] Hancock, J., Watson-Lamprey, J., Abrahamson, N. A., Bommer∗, J. J., Markatis, A., McCOYH, E., and Mendis, R., 2006, "AN IMPROVED METHOD OF MATCHING RESPONSE SPECTRA OF RECORDED EARTHQUAKE GROUND MOTION USING WAVELETS," J. Earthq. Eng., **10**(sup001), pp. 67–89. https://doi.org/10.1080/13632460609350629.
[8] Al Atik, L., and Abrahamson, N., 2010, "An Improved Method for Nonstationary Spectral Matching," Earthq. Spectra, **26**(3), pp. 601–617. https://doi.org/10.1193/1.3459159.
[9] Nie, J., Graizer, V., and Seber, D., 2023, "A Greedy Algorithm for Wavelet-Based Time Domain Response Spectrum Matching," Nucl. Eng. Des., **410**, p. 112384. https://doi.org/10.1016/j.nucengdes.2023.112384.
[10] Mukherjee, S., and Gupta, V. K., 2002, "Wavelet-Based Generation of Spectrum-Compatible Time-Histories," Soil Dyn. Earthq. Eng., **22**(9), pp. 799–804. https://doi.org/10.1016/S0267-7261(02)00101-X.
[11] Suárez, L. E., and Montejo, L. A., 2003, "Generacion de Registros Artificiales Compatibles Con Un Espectro de Respuesta Mediante La Transformada Wavelet," Medellın, Colombia.
[12] Suárez, L. E., and Montejo, L. A., 2005, "Generation of Artificial Earthquakes via the Wavelet Transform," Int. J. Solids Struct., **42**(21–22), pp. 5905–5919. https://doi.org/10.1016/j.ijsolstr.2005.03.025.
[13] Houston, T. W., Mertz, G. E., Costantino, M. C., and Costantino, C. J., 2010, "Investigation of the Impact of Seed Record Selection on Structural Response," *ASME 2010 Pressure Vessels and Piping Conference: Volume 8*, ASMEDC, Bellevue, Washington, USA, pp. 123–133. https://doi.org/10.1115/PVP2010-25919.
[14] Nie, J. R., Pires, J., and Dogan, S., 2019, "Understanding the Assumptions in Input Response Spectra for Seismic Time History Analyses," *Transactions of the SMiRT-25*, Charlotte, NC, USA.
[15] Bora, S. S., Scherbaum, F., Kuehn, N., and Stafford, P., 2016, "On the Relationship between Fourier and Response Spectra: Implications for the Adjustment of Empirical Ground-Motion Prediction Equations (GMPEs)," Bull. Seismol. Soc. Am., **106**(3), pp. 1235–1253. https://doi.org/10.1785/0120150129.
[16] Montejo, L. A., and Vidot-Vega, A. L., 2017, "An Empirical Relationship between Fourier and Response Spectra Using Spectrum-Compatible Times Series," Earthq. Spectra, **33**(1), pp. 179–199. https://doi.org/10.1193/060316eqs089m.

[17] Nie, J. R., Xu, J., Graizer, V., and Seber, D., 2020, "Estimating Stable Mean Responses for Linear Structural Systems by Using a Limited Number of Acceleration Time Histories," *PVP2020*, Volume 9: Seismic Engineering. https://doi.org/10.1115/PVP2020-21132.
[18] Nie, J. R., Xu, J., Graizer, V., and Seber, D., 2023, "Uncertainties in In-Structure Response Spectra Due to Uncertainties in Input Motion Amplitude and Phase Spectra," *PVP2023*, American Society of Mechanical Engineers, Atlanta, Georgia, USA, p. V007T08A016. https://doi.org/10.1115/PVP2023-105307.
[19] Vidot-Vega, A. L., and Montejo, L. A., 2025, "Seismic Input Minimum Power Spectral Density Compliance Effect on in Structure Response Spectra," *PVP2025*, Montreal, Quebec, Canada.
[20] (ASCE), A. S. of C. E., 2021, *Minimum Design Loads and Associated Criteria for Buildings and Other Structures*, American Society of Civil Engineers, Reston.
[21] Boore, D. M., 2010, "Orientation-Independent, Nongeometric-Mean Measures of Seismic Intensity from Two Horizontal Components of Motion," Bull. Seismol. Soc. Am., **100**(4), pp. 1830–1835. https://doi.org/10.1785/0120090400.
[22] Montejo, L. A., 2021, "Response Spectral Matching of Horizontal Ground Motion Components to an Orientation-Independent Spectrum (RotDnn)," Earthq. Spectra, **37**(2), pp. 1127–1144. https://doi.org/10.1177/8755293020970981.
[23] Rivera-Figueroa, A., and Montejo, L. A., 2022, "Spectral Matching RotD100 Target Spectra: Effect on Records Characteristics and Seismic Response," Earthq. Spectra, **38**(2), pp. 1570–1586. https://doi.org/10.1177/87552930211049259.
[24] Montejo, L. A., 2026, "Generation of Fourier Amplitude Spectra and Power Spectral Density Functions Compatible with Orientation-Independent Design Spectra for Bidirectional Seismic Analyses of Nuclear Facilities," Nucl. Eng. Technol., **58**(5), p. 104136. https://doi.org/10.1016/j.net.2026.104136.
[25] Wilson, E. L., 2002, *Three-Dimensional Static and Dynamic Analysis of Structures : A Physical Approach with Emphasis on Earthquake Engineering*, Berkeley, California : Computers and Structures, Inc.
[26] Suarez, L. E., and Montejo, L. A., 2007, "Applications of the Wavelet Transform in the Generation and Analysis of Spectrum-Compatible Records," Struct. Eng. Mech., **27**(2), pp. 173–197.
[27] Boore, D. M., Stewart, J. P., Seyhan, E., and Atkinson, G. M., 2014, "NGA-West2 Equations for Predicting PGA, PGV, and 5% Damped PSA for Shallow Crustal Earthquakes," Earthq. Spectra, **30**(3), pp. 1057–1085. https://doi.org/10.1193/070113EQS184M.
[28] Boore, D. M., and Kishida, T., 2017, "Relations between Some Horizontal-Component Ground-Motion Intensity Measures Used in Practice," Bull. Seismol. Soc. Am., **107**(1), pp. 334–343. https://doi.org/10.1785/0120160250.
[29] Afshari, K., and Stewart, J. P., 2016, "Physically Parameterized Prediction Equations for Significant Duration in Active Crustal Regions," Earthq. Spectra, **32**(4), pp. 2057–2081. https://doi.org/10.1193/063015EQS106M.
[30] Ancheta, T. D., Darragh, R. B., Stewart, J. P., Seyhan, E., Silva, W. J., Chiou, B. S.-J., Wooddell, K. E., Graves, R. W., Kottke, A. R., Boore, D. M., Kishida, T., and Donahue, J. L., 2014, "NGA-West2 Database," Earthq. Spectra, **30**(3), pp. 989–1005. https://doi.org/10.1193/070913EQS197M.
[31] Konno, K., and Ohmachi, T., 1998, "Ground-Motion Characteristics Estimated from Spectral Ratio between Horizontal and Vertical Components of Microtremor," Bull. Seismol. Soc. Am., **88**(1), pp. 228–241. https://doi.org/10.1785/BSSA0880010228.
[32] Montejo, L. A., Kottke, A. R., and Boore, D. M., 2026, "On the Computation of Orientation Independent FAS and PSD," *13th National Conference on Earthquake Engineering*, Portland, Oregon.
[33] Grant, D. N., and Diaferia, R., 2013, "Assessing Adequacy of Spectrum-matched Ground Motions for Response History Analysis," Earthq. Eng. Struct. Dyn., **42**(9), pp. 1265–1280. https://doi.org/10.1002/eqe.2270.

[34] Montejo, L. A., 2025, “Generation of Response Spectrum Compatible Records Satisfying a Minimum Power Spectral Density Function,” Earthq. Eng. Resil., **4**(2), pp. 215–228. https://doi.org/10.1002/eer2.70008.
[35] Manea, E. F., Bora, S. S., Hutchinson, J. A., and Kaiser, A. E., 2024, “Uniformly Processed Fourier Spectra Amplitude Database for Recently Compiled New Zealand Strong Ground Motions,” Seismol. Res. Lett., **95**(1), pp. 239–252. https://doi.org/10.1785/0220230228.
[36] Buckreis, T. E., Brandenberg, S. J., Mohammed, S., Nweke, C. C., Shams, R., Bahrampouri, M., Bradley, B. A., Huang, J.-Y., Kishida, T., Lanzano, G., Li, M., Luzi, L., Pajaro Miranda, C., Zimmaro, P., Bozorgnia, Y., Donahue, J. L., and Stewart, J. P., 2025, “Regional Data Sets Included in the NGA-West3 Ground Motion Database,” *Geo-Extreme 2025*, American Society of Civil Engineers, Long Beach, California, pp. 281–289. https://doi.org/10.1061/9780784486504.028.